Threshold K-LL Auger spectra of P in InP

Honghong Wang,[1] Joseph C. Woicik,[2] Teijo Åberg,[3] Mau Hsiung Chen,[4] Alberto Herrera-Gomez,[5] Tom Kendelewicz,[5] Anna Mäntykenttä,[6] Ken E. Miyano,[7] Stephen Southworth,[8] and Bernd Crasemann[1]

[1]*Department of Physics, University of Oregon, Eugene, Oregon 97403*

[2]*Materials Science and Engineering Laboratory, National Institute of Standards and Technology, Gaithersburg, Maryland 20899*

[3]*Laboratory of Physics, Helsinki University of Technology, SF-02150 Espoo, Finland*

[4]*High-Temperature Physics Division, Lawrence Livermore National Laboratory, Livermore, California 94550*

[5]*Stanford Electronics Laboratories, Stanford University, Stanford, California 94305*

[6]*Department of Physics, University of Oulu, SF-90570 Oulu, Finland*

[7]*Department of Physics, Brooklyn College, Brooklyn, New York 11210*

[8]*Physics Laboratory, National Institute of Standards and Technology, Gaithersburg, Maryland 20899*

(Received 16 March 1994)

The evolution of K-$L_{2,3}L_{2,3}\,{}^1D_2$ radiationless resonant Raman scattering into Auger-electron emission was studied by tuning synchrotron radiation across the K edge of P in InP. The spectrum can be interpreted in terms of a two-component model that involves excitation of a photoelectron (1) into a discrete excitonlike state and (2) into the continuum; extra-atomic relaxation is taken into account. Auxiliary studies of above-threshold Auger and photoelectron spectra arising from K photoionization were used to identify the dominantly atomic features of these spectra.

PACS number(s): 32.80.Hd, 32.80.Fb

I. INTRODUCTION

The escape of an electron from an inner shell of an atom involves complex dynamics of electron excitations with multiple correlational aspects [1,2] which take on added features when the atom is part of a molecule or solid and extra-atomic influences come into play [3–9]. Drastic changes in rearrangement take place when a hole state is excited near threshold [10] where excitation and decay can occur in a single second-order quantum process [11]. These phenomena can be studied fruitfully by utilizing the high intensity, monochromaticity, and tunability of synchrotron radiation to create specific inner-shell vacancies [12]. Since such vacancy states are deexcited predominantly through radiationless processes, Auger spectrometry constitutes an effective diagnostic tool to investigate these phenomena [13,14].

In free atoms, Auger spectrometry makes it possible to probe discrete and continuous features of electron-electron correlation [15,16]. In molecules [17], potential curves of doubly charged ions can be studied that involve dramatic vibrational and dissociative effects [18,19]. In solids, Auger-electron spectrometry provides site-selective information on density of states, including electron-electron correlation effects in the valence band [20]. Furthermore, Auger spectrometry in the 100-eV electron-energy range is selectively sensitive to surface phenomena [21].

In open-shell atoms, Auger spectra generally display a multiplet structure of considerable complexity, enhanced by the two holes in the final state. It is of special interest to study such spectra, as yet incompletely explored, because they reveal significant anisotropic correlation effects [16] and pertain to constituent atoms of important semiconductor materials, such as InP.

In the present exploratory study, we have measured the K-LL spectra of P in InP, excited with synchrotron radiation in the K-shell ionization threshold region and at high excess energies. The P 1s photoelectron spectrum was measured as well, in order to obtain auxiliary information on core-hole lifetimes. The spectra were analyzed with special attention to the effects of extra-atomic relaxation and of threshold resonances. The analysis makes it possible to distinguish clearly between effects of atomic origin and those due to solid-state influences, which are shown to be describable in terms of a quasiatomic screening model.

Electron- and x-ray-excited Auger spectra of P in various substances have been reported [22–31]. The only other studies to our knowledge, however, of solid-state Auger spectra excited in the threshold region with synchrotron radiation are those of Elango *et al.* [32] and of Drube, Lessman, and Materlik [33]. The latter authors measured radiationless resonant Raman scattering at the L_3 edge of 4d transition metals. These authors' results on the L_3-$M_{4,5}M_{4,5}$ Auger spectra of Rh and Pd are qualitatively similar to the present ones on P, and in general accord with the theory of radiationless resonant Raman scattering [11]. As shown below there are, however, substantial differences due to the different types of bonding. Whereas Rh and Pd are transition metals with face-centered cubic structures, InP is an A^3B^5 semiconductor with zinc-blende structure [34,35]. A delicate difference consequently arises between bonding features in the spectra. These findings may prove to be of some relevance in Auger-electron spectrometry of semiconductors and point toward new possibilities of using synchrotron radiation in this type of research.

II. EXPERIMENTAL APPROACH

Measurements were carried out both at the National Synchrotron Light Source (NSLS) in the Brookhaven Na-

tional Laboratory and at the Stanford Synchrotron Radiation Laboratory (SSRL). In the former facility, the experiments were performed on the high-resolution x-ray spectroscopy synchrotron-radiation beamline X-24A, a large-aperture device in which a collimating premirror collects 9 mrad horizontally and most of the vertical spread of x radiation from a NSLS bending magnet; this mirror preferentially absorbs unwanted high-energy x rays [36]. A schematic representation of the apparatus is shown in Fig. 1. Photons in a narrow energy band are selected by means of a fixed-exit double-crystal monochromator equipped with Si crystals in the parallel $(n,-n)$ position, followed by a focusing postmirror. A (Gaussian) photon-energy bandwidth estimated at ~ 0.66 eV full width at half maximum (FWHM) at the P K edge (~ 2150 eV) is attained from two (111) reflections. The photon flux emerging from the monochromator was monitored by measuring the electron current emitted by a gold grid placed in the x-ray beam.

In the work at SSRL, synchrotron radiation from the SPEAR (Stanford Positron-Electron Accelerator Ring) electron storage ring was used; radiation reflected from a double-focusing toroidal x-ray mirror was energy selected by two Si(111) Bragg reflections in the constant-deviation "JUMBO" double-crystal monochromator [37], with a photon-energy bandwidth of ~ 1 eV FWHM at 2150 eV.

Clean sample surfaces were prepared by cleavage of a 5×5 mm^2 bar of n-type InP along the (110) direction *in situ* in an ultrahigh-vacuum chamber ($\sim 2\times 10^{-10}$ torr) which houses a double-pass cylindrical-mirror electron-energy analyzer (CMA). Electron spectra were recorded with x rays impinging upon the sample at glancing incidence, i.e., with the polarization vector of the incident radiation aligned close to the normal to the sample surface.

Two types of absorption spectra were measured: bulk sensitive and surface sensitive. The bulk-sensitive absorption spectra were collected by the "total electron-yield" method: the InP sample was electrically isolated from the chamber; a wire connected to the sample was brought out of the chamber by a feedthrough and the bulk photoelectron current was recorded after amplification. The surface-sensitive absorption spectra were recorded by setting the CMA on a fixed electron kinetic energy of 117 eV (the diagram peak of the L-VV spectrum); the incident-photon energy was swept through the P 1s threshold region while the electron current from the Spiraltron electron multiplier in the CMA was recorded in the pulse-counting mode. Absorption spectra are shown in Fig. 2.

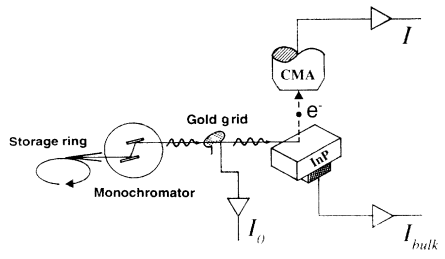

FIG. 1. Experimental layout for measuring electron spectra by recording the CMA current I in the pulse-counting mode. Bulk-sensitive absorption spectra were measured by recording the sample current I_{bulk}; surface-sensitive absorption was measured by recording I with the CMA set on L-VV Auger electrons. Results were normalized to the total photon flux proportional to the grid current I_0.

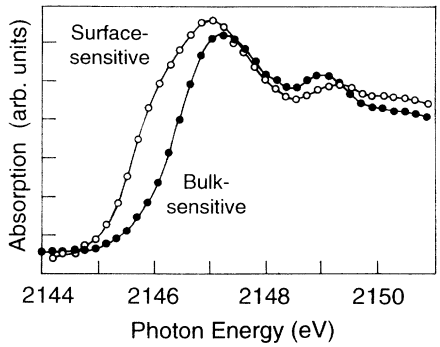

FIG. 2. Bulk- and surface-sensitive K absorption spectra of P, as functions of (uncorrected) photon energy.

K-LL and L-VV Auger spectra and P 1s photoelectron spectra were measured with the CMA in the retarding-field mode, with its large x-ray photoemission spectroscopy (XPS) aperture, at 25 and 10 eV pass energy, respectively. All spectra were normalized to incident-photon flux before analysis. A commercial nonlinear least-squares curve-fitting program was used for the analysis. This program can handle as many as eight individual components (curve functions) simultaneously. For the K-LL spectra, a linear background function was assumed over the narrow scan region of ~ 12 eV. For the L-VV Auger and P 1s photoelectron spectra, the background was fitted with the sum of a linear and an exponential function, in order to accommodate the steep slope of the secondary-electron tail. Interpretation of the L-VV and surface-sensitive absorption [38,39] spectra will be discussed in a forthcoming publication.

III. THE K-LL AUGER SPECTRUM IN THE DIAGRAM REGIME

A. Energies and coupling

It is well known that the energies and intensities of radiationless transitions can be exceedingly sensitive to the details of the atomic model, including the coupling scheme [13,15]. In particular, for K-LL spectra, the $2p^4\,{}^3P_{0,1,2}$ final states are not connected to the initial state in pure LS coupling which is approached in the lightest atoms, because parity and total orbital angular momentum cannot be conserved simultaneously in these transitions [40–42]. In intermediate coupling, mixing due to the spin-orbit interaction opens these channels.

In K-LL transitions of P, multiplet structure comes into play in both the initial and final states. The ${}^4S_{3/2}$ ground state of the neutral P atom splits into ${}^5S_2(J=2)$

and $^3S_1(J=1)$ levels in singly ionized P^+ with a 1*s* hole. The latter state lies approximately 1 eV below the former. A similar situation was recently demonstrated in atomic oxygen, where the ^3P ground state splits into ^4P and ^2P levels in the O^+ 1*s*-hole state, resulting in two distinct *K-LL* Auger series [43].

We have performed relativistic computations in intermediate coupling of the K-$L_{2,3}L_{2,3}$ spectrum for *free* P atoms, using the multiconfiguration Dirac-Fock (MCDF) method [44]. The details of this self-consistent-field approach have been described by Chen [45]. The Breit interaction was taken into account by including the frequency-dependent Breit operator [46] in the Hamiltonian, thus incorporating the magnetic and retardation contributions to the level energies [45]. Self-energy and vacuum polarization, the two main radiative corrections from quantum electrodynamics (QED), were included in the energy calculations as previously described [47,48]. Inclusion of the Breit and QED corrections reduces the calculated Auger energies, e.g., from 1839.1 to 1837.4 eV for the dominant K-LL $^1D_2$ line of free P. Results for the more intense transitions from the present MCDF calculations are listed in Table I. The uncertainty of these calculated energies is estimated to be approximately ± 1 eV, resulting mostly from some correlation effects that were neglected.

The accuracy of the theoretical free-atom intermediate-coupling MCDF energies can be tested by comparing results for Ar, calculated in the same manner, with high-resolution measurements. Differences between the present theoretical and the experimental [49] Ar K and $L_{2,3}$ binding energies are approximately 0.7 eV. After cancellations, the error in calculated *Auger* energies is approximately ± 0.7 eV for K-$L_{2,3}L_{2,3}$ transitions. This conclusion is supported by comparison of measured [50] and calculated MCDF *K-LL* Auger energies of Ar (Table II).

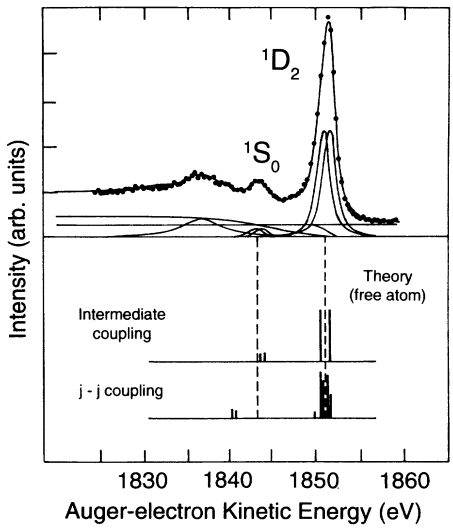

FIG. 3. Measured P K-$L_{2,3}L_{2,3}$ Auger spectrum excited above the K edge ($h\nu=2193$ eV), compared with theoretical calculations in intermediate and *j-j* coupling; heights of the vertical bars are proportional to integrated intensities. The experimental spectrum is decomposed by means of the PEAKFIT program. The smoothed step functions simulate the background; the broad Voigt function at 1837 eV represents the plasmon loss. Decomposition of the Auger multiplets is described in the text.

Predicted energies and line-intensity ratios are very sensitive to the coupling, even for such a light atom as P. For example, the calculated K-$L_{2,3}L_{2,3}$ $^1D_2$:$^1S_0$:$^3P_{0,1,2}$ intensity ratio is 100:8:3 in *j-j* coupling, while it is 100:14:9 in intermediate coupling (Table I). The measured $^1D_2$:$^1S_0$ ratio is 100:(14.3±1.0) (Fig. 3); the ^3P peak is too weak and broad, due to splitting, to be resolved in the

TABLE I. Multiconfiguration Dirac-Fock K-$L_{2,3}L_{2,3}$ Auger-electron energies and intensities for P, calculated in intermediate coupling.

Final state	Initial state	Auger energy (eV)	Intensity (ma.u.)	Relative intensity (%)
$2p^4(^1D_2)$	$1s3p^3(^4S)^5S_2$	1836.93	3.28	16.7
		1836.89	2.42	12.3
		1836.87	1.59	8.1
		1836.86	0.79	4.0
	$1s3p^3(^4S)^3S_1$	1838.02	3.27	16.6
		1837.99	2.42	12.3
		1837.97	1.59	8.1
		1837.96	0.79	4.0
$2p^4(^1S_0)$	$1s3p^3(^4S)^3S_1$	1831.75	1.10	5.6
	$1s3p^3(^4S)^5S_2$	1830.65	1.10	5.6
$2p^4(^3P_{0,1,2})$	$1s3p^3(^4S)^5S_2$	1841.31	0.27	1.3
		1841.40	0.42	2.1
	$1s3p^3(^4S)^3S_1$	1842.50	0.42	2.1
		1842.41	0.27	1.3
		Total[a]	19.72	100

[a]The lines with intensities lower than 0.02 ma.u. are not listed here. The unlisted transitions account for less than 2% of the total K-$L_{2,3}L_{2,3}$ intensity.

TABLE II. Comparison of measured Ar K-$L_{2,3}L_{2,3}$ Auger energies with MCDF predictions in intermediate coupling.

Final state	Calculated energy (eV)	Measured energy[a] (eV)
$^3P_2$	2669.6	2669.1
$^3P_0$	2667.4	2666.9
$^1D_2$	2660.8	2660.5
$^1S_0$	2652.2	2650.9

[a]Reference [50].

measured spectra. The measured ratio agrees with the intermediate-coupling prediction, verifying the equal importance of electrostatic and spin-orbit interaction energies at this low atomic number. This observation is in accord with a measurement of the K-LL spectrum of elemental red phosphorus by Schärli and Brunner [22], who found excellent agreement between observed line intensities and those calculated in intermediate coupling with configuration interaction [51].

The observed energy splitting between the $^1D_2$ and $^1S_0$ groups, however, is 7.5±0.1 eV (Fig. 3); this result falls between the calculated splitting of 9.6 eV in j-j coupling and 6.2 eV in intermediate coupling with limited configuration interaction (Table I), but agrees well with a measurement (7.7±0.4 eV) [22] that was recently confirmed [29]. The calculations are for free atoms, but the splitting should not be significantly affected by the solid-state environment because the extra-atomic relaxation energy (cf. Sec. III B) is, in first order, the same for Auger transitions that lead to the same final two-hole state. This energy discrepancy is thus most likely due to lack of correlation in our calculations. We include the standard $2p^4(^1S)$-$2s^0(^1S)$ mixing but neglect the configuration interaction of $2s^22p^4(^1S,^1D)$ with $2p^4(^1S,^1D)(2snd\,^1D)^1D,^1S$, $2s^22p^53s^03p^3np,f$, $2s^22p^53s^23p^1np,f$, and $2s^22p^53s3p^2nd$. According to Table II, there is a similar discrepancy in the case of Ar: the measured splitting is 9.6 eV, while the calculated splitting is 8.6 eV.

The splitting among lines within the $^1D_2$ and $^1S_0$ groups caused by separation between the initial $^5S_2(J=2)$ and $^3S_1(J=1)$ levels, referred to above, is reflected in the calculated energies in Table I. The relative population of the initial states was treated as unknown. A statistical ratio of 5:3 would be expected between the $J=2$ and $J=1$ initial states if the atoms were free and randomly oriented and pure LS coupling governed the final states in the photoionization. However, the states are subject to intermediate coupling with configuration interaction and pertain to atoms in the solid; these circumstances invalidate the $\frac{5}{3}$ rule. In the measured spectra, a good fit was obtained with two Lorentzians of equal intensity. The splitting was barely resolvable. The spectrum shown in Fig. 3 was measured at SSRL with a CMA resolution of $\simeq 1$ eV; it shows a splitting that does not exceed 0.6±0.1 eV between the $J=2$ and $J=1$ components. An identical result was obtained in a measurement at NSLS with $\simeq 0.5$ eV CMA resolution and a narrower scan. The observed splitting is less than the theoretical prediction of 1.1 eV for free P atoms (Table I). The difference may be due to variation of the intensity ratio, reflecting the unknown initial-state population.

B. Widths and transition rates

The theoretical 1s K-LL Auger transition rate for free P atoms, calculated in intermediate coupling with configuration interaction [51], is 14.925 ma.u., which corresponds to a partial width of 0.406 eV. We add 23.4% for K-LM transitions [52] and find a total theoretical K-level width $\Gamma_A(1s)=0.501$ eV. The calculated radiative K width is $\Gamma_R=0.033$ eV [53], whence the calculated total K-level width of P is $\Gamma(1s)=0.533$ eV.

A partial check on this result is provided by the fact that the ensuing theoretical K-shell fluorescence yield is $\omega\equiv\Gamma_R/(\Gamma_R+\Gamma_A)=0.062$, in good agreement with the measured K fluorescence yield $\omega_K=0.060\pm0.003$ of P in PH_3 [54].

The experimental K-level width of P in InP can be deduced from 1s photoelectron spectra [Fig. 4(a)]. Such

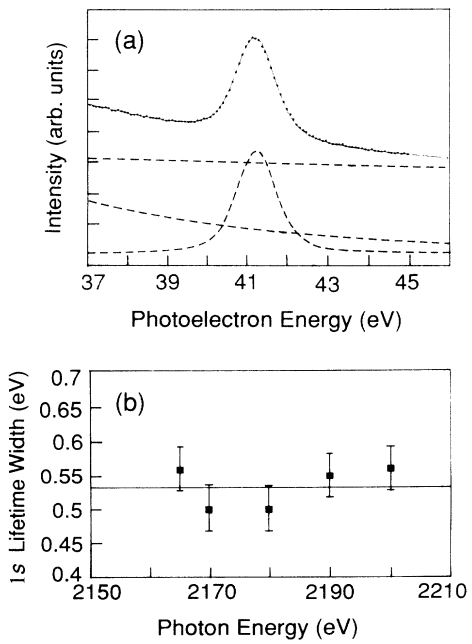

FIG. 4. (a) Decomposition of the 1s photoelectron spectrum into a Voigt line-shape function and the background function given by Eq. (1); linear and exponential components of the background are shown separately. (b) Measured P 1s lifetime width above the K threshold, as function of (uncorrected) photon energy.

spectra, excited with x rays of energies from 2165 to 2200 eV (20 to 55 eV above threshold), were recorded with a CMA pass energy of 10 eV, giving 0.2-eV resolution. The spectra were fitted with a Voigt line shape [55,56] superimposed on a background function $f_b(\varepsilon)$ that contains linear and exponential components:

$$f_b(\varepsilon)=a+b\varepsilon+c\exp(-\varepsilon/d)\ , \tag{1}$$

where ε is the photoelectron kinetic energy and a,b,c,d are fitting parameters. This function includes a correction for the variation of electron-spectrometer transmission with retarding potential [57]. In addition to this variation of spectrometer source volume with electron energy, the background contains contributions from inelastically scattered photoelectrons that were created within the bulk of the sample [58]. Fitting of the background function (1) is delicate; it greatly influences the apparent width of the deconvoluted Lorentzian line shape.

The Voigt profile fitted to the background-subtracted peaks is a convolution of the Lorentzian natural (lifetime) line shape and a Gaussian function that serves as an approximation to the electron spectrometer function and the contribution from the energy width of the incident x-ray beam. In photoelectron spectra of semiconductors, the Gaussian width can furthermore contain a contribution from phonon broadening [56]. In the present spectra, a best fit was obtained with a Gaussian width of 0.69 ± 0.02 eV, which includes the 0.2-eV CMA resolution and a 0.66-eV x-ray width that does not vary appreciably over the range of the scans. This width is used in all calculations in Sec. IV.

Analysis of five spectra excited with x rays of different energies leads to the P 1s widths plotted in Fig. 4(b). Error bars shown on individual data points represent statistical errors from the fitting of the Voigt function as well as the uncertainty in the coefficients of the background function. The final experimental result is $\Gamma(1s)=0.53\pm0.04$ eV for P in InP. The measured width agrees closely with the theoretical 1s-level width of free P atoms (0.533 eV), discussed above. This agreement leads to the conclusion that the K-LM transition rate, which accounts for 18% of the 1s theoretical width [52], does not differ by more than $\sim 50\%$ between free P atoms and K-LV for P in InP, despite the difference between atomic M-shell wave functions and those of P valence electrons V in the crystal. The present work also confirms the P 1s width listed in the widely used tables of Krause and Oliver [59], 0.53 ± 0.03 eV, a semiempirical value derived by combining the calculated radiative width [53] with the measured fluorescence yield [54]. The close agreement between the free-atom and solid-state values of $\Gamma(1s)$ is a consequence of the localization of the 1s wave function near the nucleus, where most of the overlap with outer-shell wave functions in the transition matrix elements occurs.

A theoretical estimate of the predicted K-$L_{2,3}L_{2,3}\ ^1D_2$ linewidth can be obtained by extrapolating calculated L-MM Auger rates [60] to $Z=15$; we find $\Gamma(2p_{1/2})=0.13$ eV and $\Gamma(2p_{3/2})=0.15$ eV; the radiative widths are negligible, fluorescence yields being $\sim 10^{-4}$ [61,62]. Adding the theoretical K width of 0.533 eV, discussed above, we find a calculated free-atom width of 0.81 eV for a K-$L_{2,3}L_{2,3}\ ^1D_2$ Auger line. This result exceeds the K-$L_{2,3}L_{2,3}$ width (0.60 eV) listed in Ref. [59].

In InP, the P $L_{2,3}$ level widths are somewhat larger; a measurement by Kendelewicz *et al.* shows $\Gamma(2p_{1/2})\simeq\Gamma(2p_{3/2})=0.2\pm0.1$ eV [63], a width confirmed by Wilke *et al.* [64]. This fact indicates that the P L-VV rates in InP exceed the L-MM rates in free P atoms by $\simeq 40\%$, close to the upper limit of the solid-state K-LV rates as revealed by the K width discussed above. This estimate is contingent upon the assumption that factors other than lifetime broadening (i.e., crystal-field splitting, phonon broadening) do not contribute significantly to the measured L widths.

Our measured width of the two Lorentzian components of the $^1D_2$ K-L_2L_3 doublet (Fig. 1) is 1.1 ± 0.1 eV (FWHM). For comparison, we measured the same lines in a GaP sample; the K-LL widths there were found to be 1.0 ± 0.1 eV, with a separation which does not exceed 0.7 ± 0.1 eV between two Lorentzian peaks of equal intensity. These widths are compatible with the sum of the measured P 1s width (0.53 ± 0.04) eV plus twice the measured 0.2-eV 2p width in InP from Ref. [63].

C. Extra-atomic relaxation energy

It is well known that atomic inner-shell ionization (binding) energies in solids are generally lower than in free atoms, whereas the opposite holds for Auger-electron energies [3–7,9]. The data in Table III confirm this trend for P in InP. A central concept in the theory of solid-state shifts is the *extra-atomic relaxation energy* R^e that arises from the screening by valence or conduction electrons of an ionic core which has undergone an increase in charge by one unit.

In the following, all energy shifts Δ are defined to be positive and it is assumed that transition energies are given with respect to the vacuum level, except for quantities that do not depend on the reference level. The Auger parameter

$$\xi^s=I^s_j-I^s_k-I^s_l-(I^s_j-I^s_{kl}) \tag{2}$$

is such a quantity [5] in which I^s_ν $(\nu=j,k,l)$ are the ionization energies of electrons in subshell ν and $E^s_{jkl}=I^s_j-I^s_{kl}$ is the corresponding Auger energy in the solid (s). The quantity I^s_{kl} is the amount of energy, with respect to the vacuum level, that is required to create the holes k and l. This quantity can, however, be defined in Eq. (2) with respect to any other reference level, as long as the ionization energies I^s_ν are defined with respect to the same level. The free-atom Auger parameter ξ^a is defined analogously to ξ^s, and thus is also independent of the reference level. The extra-atomic relaxation energy then is defined as the difference between these parameters, $R^e=\xi^a-\xi^s$; a simple calculation shows that

$$R^e=\xi^a-\xi^s=\Delta_{kl}-\Delta_k-\Delta_l\ , \tag{3}$$

where $\Delta_{kl}=I^a_{kl}-I^s_{kl}$ and $\Delta_\nu=I^a_\nu-I^s_\nu$ $(\nu=k,l)$. Accord-

TABLE III. *K-LL*, *K-LV* Auger parameters ξ and extra-atomic relaxation energies R^e for P in InP. All energies are in eV.

	This work			Reference [26]		
	Calculated[a] (atom)	Measured[b] (solid)	Deduced[c]	Calculated (atom)	Measured[d] (solid)	Deduced[c]
$E_b(1s)$	2152.6	2146.3±0.7			2142.2±0.3	
$E_b(2p)$	138.8	133.3±0.7			128.85±0.3	
$E_b(3p)$	8.84	7.9±0.7				
$E_{1s2p2p}(^1D_2)$	1837.4	1853.1±0.5			1858.45±0.3	
E_{1s2p3p}	1988.5	2000.9±0.5				
$\xi^a(2p2p)$	37.6			37.23		
$\xi^a(2p3p)$	16.5					
$\xi^s(2p2p)$		26.6±1.3			26.05±0.5	
$\xi^s(2p3p)$		4.2±1.3				
$R^e(2p2p)$			11.0±1.3			11.18±0.5
$R^e(2p3p)$			12.3±1.3			

[a]All the binding energies for free atoms are calculated with the MCDF code. The Auger energy $E_{1s2p2p}(^1D_2)$ is the weighted average from Table I. Auger energy E_{1s2p3p} is calculated by using the average-level mode of the MCDF code.

[b]Energies are with reference to the analyzer vacuum level; indicated errors are statistical only. All values were obtained with the same experimental setup at SSRL. The $E_{1s2p2p}(^1D_2)$ energy is thus slightly different from that reported in Sec. III A, which was obtained earlier with much smaller data-acquisition steps.

[c]$R^e=\xi^a-\xi^s$.

[d]Energies with reference to the Fermi level.

ing to Eqs. (2) and (3), the Auger-electron energy shift $\Delta_{jkl}=E^s_{jkl}-E^a_{jkl}$ then is

$$\Delta_{jkl}=\Delta_{kl}-\Delta_j=-\Delta_j+\Delta_k+\Delta_l+R^e\ , \tag{4}$$

where $\Delta_j=I^a_j-I^s_j$ is the solid-state shift associated with the initial hole j. Because we have $\Delta_j\simeq\Delta_k$ and $R^e\gg\Delta_l$ in most solids, Eq. (4), which is exact, shows that we usually have

$$\Delta_{jkl}\simeq\Delta_l+R^e\simeq R^e\ . \tag{5}$$

The extra-atomic relaxation energy thus constitutes the dominant component of the solid-state Auger-energy shift.

Direct comparison of predicted Auger energies with measurements is encumbered by the fact that the latter depend on the reference level and charging effects in the electron-energy analyzer, which vary between individual instruments; thus the mean P K-L_2L_3 $^1D_2$-doublet energy determined with three different CMA's in the present work was found to be 1851.1±0.1 eV (SSRL-I), 1852.3±0.1 eV (NSLS), and 1853.7±0.1 eV (SSRL-II). This difficulty can be circumvented by using Eq. (2) that allows a direct determination of the extra-atomic relaxation energy from measured quantities, eliminating the contributions of charging effects and the reference levels.

To avoid ambiguity in the calculation of the free-atom Auger parameter ξ^a [23], we compute it *ab initio* by subtracting the K-L_2L_3 $^1D_2$ energy and twice the (average) $2p$ ionization energy from the $1s$ ionization energy [Eq. (2) with s replaced by a]. All three energies were computed with a relativistic self-consistent-field code [44,45]; Breit energy [47] and QED corrections [47,48] are included.

Results are summarized in Table III. For comparison we also list data on InP obtained by Franke *et al.* [26] with reference to the Fermi level, while those of the present work refer to the vacuum level. Because ξ and R^e are independent of the reference level, these parameters show good agreement between the two studies.

IV. RAMAN REGIME

The photoinduced Auger effect involves at least two outgoing electrons, the photoelectron and one Auger electron. The residual holes can be filled by electrons from outer shells or from the valence band, leading to additional radiative and radiationless transitions in the crystal. The charge of the residual ion can thus be quite high unless the ion is screened by electrons from neighboring atoms. The primary process can be viewed as resonant double photoionization mediated by a complete set of intermediate states; these correspond to an intermediate virtual inner-shell hole, which is localized at one of the atoms, and an electron in excited bound or continuum states [11,65]. As the energy $\hbar\omega$ of the incoming photons is increased, sweeping through the corresponding inner-shell threshold, continuous asymmetric electron distributions associated with different residual two-hole multiplets evolve into Auger-electron lines with characteristic energies [11]. The shapes and energies of the characteristic lines continue to change until the energy of the photoelectron exceeds that of the Auger electron. The energy region just below the threshold is usually referred to as

the resonant Raman scattering (RRS) regime, and the region above the threshold, as the postcollision interaction (PCI) regime. In these regimes the nonresonant two-electron emission amplitude is usually negligible compared with the resonant amplitude.

A useful reference quantity is the photon excess energy

$$E_{\rm exc}=\hbar\omega-(E^{(1+)}-E_0)\ , \tag{6}$$

which is given with respect to the ionization energy $I_i=E^{1+}-E_0$, where $E^{(1+)}$ is the energy of the crystal with the virtual atomic inner-shell hole in state i, and E_0 is the ground-state energy of the crystal. Thus $E_{\rm exc}\lesssim 0$ corresponds to RRS and $E_{\rm exc}\gtrsim 0$ marks the beginning of PCI [11]. In both regimes, the two excited or emitted electrons share energy in accordance with energy conservation:

$$\hbar\omega+E_0=E^{(2+)}+\varepsilon+\varepsilon_A\ . \tag{7}$$

Here, $E^{(2+)}$ is the energy of the crystal with two residual holes, ε is the energy of the photoelectron, and ε_A is the Auger-electron energy. Both ε and ε_A are thus given with respect to $I_{ff'}=E^{(2+)}-E_0$, where f and f' are the states with the residual holes. It follows from Eq. (6) that Eq. (7) can be cast in the form

$$E_{\rm exc}+\varepsilon_A^0=\varepsilon+\varepsilon_A\ , \tag{8}$$

where $\varepsilon_A^0=E^{(1+)}-E^{(2+)}$ is the nominal Auger energy. According to Eq. (8), two-electron emission becomes possible at $E_{\rm exc}=-\varepsilon_A^0$, but it is not until $E_{\rm exc}$ approaches zero that the process becomes resonant, with the photoelectron excited into an excitonlike bound state or into a low-energy conduction-band state. Because of screening, one of the continuum electrons tends to be slowed down and the other, speeded up; this PCI effect sets in gradually as $E_{\rm exc}$ increases from $-\varepsilon_A^0$ to above the threshold. As $E_{\rm exc}>0$ approaches ε_A^0 from below, the PCI effect gradually vanishes. Photoionization and Auger-electron emission can then quite accurately be treated as separate, sequential processes. Without PCI and in accordance with Eq. (8), we have $\varepsilon=E_{\rm exc}$ and $\varepsilon_A=\varepsilon_A^0$ [1,11].

In addition to the evolution of continuous RRS distributions into characteristic Auger-electron lines distorted and shifted by PCI, discrete features can appear in the spectrum as well. These features are characterized by linear dispersion with incident photon energy because, according to Eq. (7), ε_A depends linearly on $\hbar\omega$ if ε equals a fixed energy ε'. The intensity of Auger-electron emission peaks sharply at $\varepsilon_A=E'_{\rm exc}+\varepsilon_A^0-\varepsilon'$ as $E_{\rm exc}$ is tuned through some energy $E'_{\rm exc}\cong\varepsilon'$; this is the radiationless analog of resonance fluorescence. Linear dispersion and intensity enhancement of the Auger peak are thus characteristics of the formation of localized two-hole states in the solid [11].

A third characteristic of localization is a reduction of the width of the resonance Auger line corresponding to $\varepsilon=\varepsilon'$. Let Γ_s be the width of the spectral function of the incoming photon beam and Γ, the lifetime width of the virtual intermediate inner-shell hole. Then, if $\Gamma_s\lesssim\Gamma$, the width of the resonance line is governed by Γ_s rather than by Γ, in analogy to resonance fluorescence [66]. This narrowing effect has been predicted theoretically [67] and verified experimentally for both radiative [68] and radiationless [69,70] RRS in free atoms. The effect should not be confused with an apparent narrowing that occurs when the asymmetric continuous RRS distribution evolves into the normal Auger line [11,66,67].

The characteristic discrete energies ε' of localized two-hole states in a solid can be either negative or positive. These energies are usually negative for excitonlike bound states. It is possible, however, for ε' to be positive if a potential barrier is formed at the site of the two holes, due to neighboring atoms. A quasi bound state of this type has an energy ε' below the top of the barrier and is characterized by a large wave-function amplitude inside the barrier. Inner-shell absorption spectra of positive ions in ionic crystals have been interpreted in terms of such barriers [71]; other solid-state applications exist as well [72,73].

The features described above are characteristic of threshold excitation of inner-shell holes in any material. It has been shown that a generalization of time-independent resonant scattering theory to two-particle emission permits a unified treatment of both radiative and radiationless RRS, including PCI [11,65]. Computations based on this theory have been performed for free atoms, leading to quantitative and experimentally confirmed predictions of features discussed above, including more subtle ones such as recapture of the photoelectron [74] and shake of a Rydberg electron in Auger-electron emission [75]. For solid-state systems there are no comparable calculations, but we show below that even qualitative considerations based on the outline above can lead to interesting conclusions.

The K-$L_{2,3}L_{2,3}$ Auger spectrum of P in InP, shown in Fig. 3, was excited with a photon energy 50 eV above the K threshold. In the present section we examine the evolution of the K-$L_{2,3}L_{2,3}$ $^1D_2$ RRS into the corresponding Auger line of this spectrum as the energy of the exciting photons is tuned through the K threshold. In our discussion of the threshold spectrum we define an approximate photon excess energy $E_{\rm exc}$ [Eq. (6)] with respect to the energy of the inflection point of the continuous part of the bulk K absorption spectrum shown in Fig. 6(b) and discussed below. We take this energy to be the binding energy of a P K electron in InP, equal to $I_{1s}=2142.2\pm0.3$ eV with respect to the Fermi level [26]. It will be shown below that the integrated intensity of the K-LL signal can be resolved into a discrete and a continuous part, which mimic the bulk rather than the surface absorption spectrum [39] as a function of the photon excess energy.

A. Two-component analysis of the K-LL threshold spectrum

Figure 5 shows experimental K-$L_{2,3}L_{2,3}$ $^1D_2$ spectra for both negative and positive photon excess energies $E_{\rm exc}$. The background was taken to be linear in the narrow range of observed electron energies. The spectra were resolved into components using a minimum number of assumptions, along the following steps.

(i) The intermediate- and final-state multiplet and possible crystal-field splittings were neglected.

(ii) The spectra show a rather symmetric sideband or satellite which moves toward higher electron energies as E_{exc} increases. The position of the satellite is indicated by arrows in Fig. 5; it was assumed that the satellite exists also for $E_{exc}<0$.

(iii) From the positive excess-energy data a Voigt profile was assigned to this satellite, with a FWHM of $\Gamma_r=1.06\pm0.01$ eV. The satellite was assumed to have the same form for $E_{exc}<0$.

(iv) It was found that for positive excess energies the remaining structure could also be represented by a Voigt profile, but with a larger width of $\Gamma_m=1.28\pm0.04$ eV. Below $E_{exc}=0$ this structure was found to be very asymmetric; it was fitted with an asymmetric double sigmoidal function.

(v) In the fitting functions, the positions and heights of the maxima of the two components were optimized; the result was an excellent representation of the measured spectra.

Figure 5 and the fit show that the main line emerges into the normal K-$L_{2,3}L_{2,3}$ $^1D_2$ Auger line at $E_{exc}\gtrsim 5$ eV and that the resonant satellite line vanishes on both sides of $E_{exc}=0$. Detailed results are presented in Fig. 6. Figure 6(a) shows that the *integrated intensities* of the main and resonance lines display distinctly different behaviors as functions of $\hbar\omega$ or E_{exc}. The FWHM of the resonance intensity curve in Fig. 6(a) is $\Gamma_r'=1.6\pm0.5$ eV. The intensity of the normal line exhibits some fluctuations with photon energy that correlate with the structure of the bulk K absorption curve. In fact, as shown in Fig. 6(b), the *sum* of the two integrated intensities follows the absorption spectrum extremely well. In Fig. 6(c) we plot the dependence of the energy of the resonance peak on $\hbar\omega$. According to Eq. (7), this dependence should be linear if the resonance peak corresponds to a discrete excitation of one electron. As shown in the figure, the solid curve with unit slope agrees very well with the experimental points. This result, together with the resonant intensity behavior shown in Fig. 6(a), unambiguously identifies the existence of a discrete excitation in K-LL $^1D_2$ resonant Raman scattering by P in InP.

There even is an indication of line narrowing. In the Raman regime, the K-LL spectra were taken with a

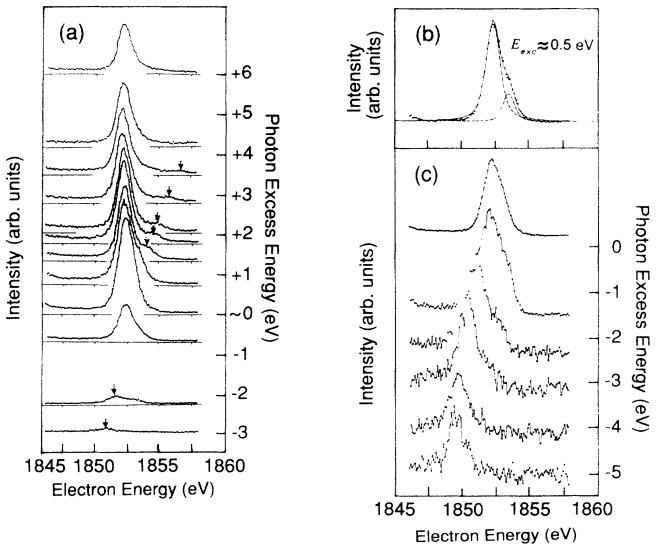

FIG. 5. (a) Evolution across the K threshold of P K-$L_{2,3}L_{2,3}$ $^1D_2$ resonant Raman scattering into the corresponding Auger line. Arrows indicate the positions of some resonant Raman peaks in spectra measured at various approximate photon excess energies (indicated on the right). (b) Two-component decomposition of the spectrum at $E_{exc}=0.5$ eV, after subtraction of a linear background. (c) Enlargement of K-$L_{2,3}L_{2,3}$ $^1D_2$ spectra measured with E_{exc} in the range from approximately -5 to $+0.2$ eV. The sequence shows the asymmetrical shape of the normal Raman peaks which with increasing E_{exc} evolve into the Auger line.

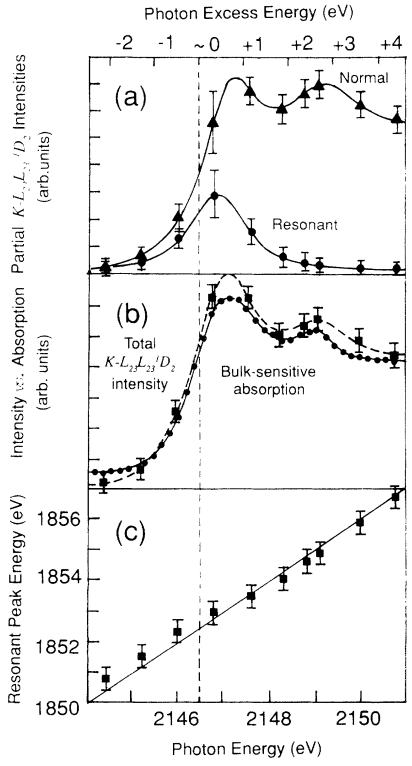

FIG. 6. (a) Integrated intensities of the two components in the resonant Raman scattering spectra shown in Fig. 5, as functions of approximate photon excess energy (top scale). Dots represent the resonance line and triangles, the normal line. Solid curves through the data have been drawn to guide the eye. (b) The sum of resonant and normal intensities from Fig. 6(a), which represents the total integrated K-$L_{2,3}L_{2,3}$ $^1D_2$ intensity (dashed curve through squares), compared with the bulk-sensitive K absorption spectrum (solid curve through dots). (c) Energy of the resonant peak in the Raman spectrum, as a function of photon excess energy. The solid line represents the best fit to the data points of a straight line with unit slope, indicating linear dispersion.

CMA resolution of $\simeq 0.8$ eV. The small initial-state splitting of the ^1D line could be neglected and the peaks were fitted to a single Voigt line shape, after linear background subtraction. The width of the resonance line was determined at photon energies near $\hbar\omega = 2149$ eV, where the resonance and normal lines can be resolved clearly; here, the Voigt width of the resonance line was found to be 1.06 ± 0.10 eV. The Voigt width thus determined was used also for the resonance line in the analysis of spectra in which this line could not be resolved from the normal line; the width and asymmetry of the normal line were allowed to float freely in the fitting procedure. The Voigt width of the normal line was thus found to reach a minimum of 1.1 ± 0.1 eV near $\hbar\omega = 2146.8$ eV; it increases to 1.54 ± 0.10 eV at $\hbar\omega = 2200$ eV. The narrowing of the resonance line is due to the fact that the intermediate-state lifetime width is suppressed when the incident-photon spectral function is comparable to or narrower than the 1*s* hole-state lifetime width (Sec. IV B).

B. Interpretation of the two-component structure

The salient features of the observed spectrum can be explained by a formula previously used for the interpretation of PCI, including photoelectron recapture and shake of a Rydberg electron during Auger decay of free atoms [11,69,74,75]. The equation essentially follows from the exact resonant-scattering description [65] of two-electron emission by treating the final-state interactions to lowest order [76]. We have, in atomic units, for the partial doubly differential cross section per unit photon energy,

$$F = F(\omega, \varepsilon_A, \varepsilon) = \frac{d}{d\omega}\left[\frac{d^2\sigma}{d\varepsilon\, d\varepsilon_A}\right] = \frac{4\pi\alpha\omega}{3}\Gamma(\varepsilon_A)|\langle\varepsilon|\tau_i\rangle|^2 N(\omega-\omega_0)\frac{dN_f}{d\varepsilon_A} . \quad (9)$$

Here, $\Gamma(\varepsilon_A)$ is the Auger decay probability. In the overlap integral $\langle\varepsilon|\tau_i\rangle$, $|\varepsilon\rangle$ is the wave function of the discrete or continuum excited electron, evaluated in the field of the residual doubly charged ion with two holes, and

$$|\tau_i\rangle = \int_{\varepsilon_i}^{\infty} \frac{|\tau\rangle\langle\tau\|r\|0\rangle d\tau}{\omega - I_i - \tau + i\Gamma_i/2} \quad (10)$$

describes the influence of the virtual intermediate hole with lifetime width Γ_i and ionization energy I_i. The photon excess energy $E_{\rm exc}$, previously defined in Eq. (6), thus is $E_{\rm exc} = \omega - I_i$. The wave function $|\tau\rangle$ must be evaluated in the field of the singly charged ion with the intermediate hole *i* and can be either discrete or continuous. The integration in Eq. (10) therefore includes a summation over discrete states, as indicated by the lower limit ε_i which can be negative. The matrix element $\langle\tau\|r\|0\rangle$ is the reduced dipole matrix element between the ground-state wave function $|0\rangle$ and $|\tau\rangle$.

The wave functions $|\varepsilon_a\rangle$, $|\varepsilon\rangle$, and $|\tau\rangle$ should be consistent with the point group symmetry of the crystal field and selection rules. In the case of phosphorus in InP, which is an A^3B^5 semiconductor with zinc-blende structure, the symmetry group is T_d. In Eq. (9) we have ignored any crystal-field splitting effects because the final holes are in the $L_{2,3}$ shell of P and the virtual hole is in the *K* shell. The change of charge by one unit between the intermediate and final cores induces phonon broadening [4] which we also neglected. According to the continuum model, the broadening would be of the order of 0.1 eV.

The spectral function $N(\omega-\omega_0)$ in Eq. (9) (normalized to unity) describes the distribution of the number of photons per unit energy in the beam, centered at $\omega = \omega_0$. The influence of the final-double-hole-state lifetime $\Gamma_{ff'}^{-1}$ is described by the normalized density function

$$\frac{dN_f}{d\varepsilon_A} = \frac{\Gamma_{ff'}/2\pi}{(\omega-\varepsilon-\varepsilon_A-I_{ff'})^2+\Gamma_{ff'}^2/4} , \quad (11)$$

where $I_{ff'}$ is the energy required to remove the two electrons from the states *f* and *f'*, respectively. Both I_i and $I_{ff'}$ are taken with reference to the Fermi level.

We need to consider the quantities

$$I(\varepsilon_A, \omega_0) = \int_0^{\infty}\int_{\varepsilon'}^{\infty} F(\omega, \varepsilon_A, \varepsilon)\, d\varepsilon\, d\omega , \quad (12)$$

which gives the shape of the electron-energy spectrum for a given ω_0 and

$$I(\omega_0) = \int_0^{\infty} I(\varepsilon_A)\, d\varepsilon_A , \quad (13)$$

which gives the integrated intensity of this spectrum as a function of ω_0. Comparison with the experimental results in principle requires a convolution of $I(\varepsilon_A, \omega_0)$ with the spectrometer function $S(\varepsilon)$ of the CMA. In the following qualitative analysis, however, we take *S* into account approximately by using an effective $N(\omega-\omega_0)$ that is assumed to have been convoluted with *S*; this procedure slightly widens the spectral function.

(a) Main line. The gross features of the evolution of the continuous ("*c*") RRS structure into the K-$L_{2,3}L_{2,3}$ $^1D_2$ Auger line can be inferred from Eq. (9) by neglecting the PCI effect which, while it exists both below and above the *K* threshold, is of minor importance in this context. This approximation amounts to setting $\langle\varepsilon|\tau\rangle = \delta(\varepsilon-\tau)$ in the factor $\langle\varepsilon|\tau_i\rangle$. Physically it implies neglect of shakeup or shakedown processes in the continuum (conduction band) resulting from the change of core charge by one unit. We have

$$I_c(\varepsilon_A, \omega_0) = \int_{-I_{1s}}^{\infty}\int_{-E_{\rm exc}}^{\infty} \frac{\Gamma(\varepsilon_A)\sigma_c(x+E_{\rm exc})N(E_{\rm exc}-E_{\rm exc}^0)(\Gamma_{2p2p}/2\pi)\, dE_{\rm exc}\, dx}{(x^2+\Gamma_{1s}^2/4)[(\varepsilon_A^0-\varepsilon_A-x)^2+\Gamma_{2p2p}^2/4]} , \quad (14)$$

where $x=\varepsilon-E_{\rm exc}$ and $\sigma_c=\sigma_c(x+E_{\rm exc})$ is the 1*s* photoionization cross section of P *excluding* any discrete features. In Eq. (14) we have inserted the explicit expression (11) for $dN_f/d\varepsilon_A$, which approaches $\delta(\varepsilon_A^0-\varepsilon_A-x)=\delta(\omega-\varepsilon-I_{2p2p})$ as $\Gamma_{2p2p}\to 0$.

It can be assumed that the radiationless decay probability $\Gamma(\varepsilon_A)$ is nearly constant and equal to the decay probability $\Gamma(\varepsilon_A^0)$ of the K-$L_{2,3}L_{2,3}$ $^1D_2$ line in the near-K-edge region of photon excess energies (Fig. 5). This situation is thus analogous to the evolution of radiative K-L RRS into $K\alpha$ fluorescence [67]. The radiative decay probability Γ_R, corresponding to $\Gamma(\varepsilon_A^0)$, is exactly constant, and Γ_{2p2p} and I_{2p2p} in Eq. (14) need to be replaced by Γ_{2p} and I_{2p}, respectively, in the radiative case. The evolution of the continuous Auger K-LL RRS into the K-$L_{2,3}L_{2,3}$ $^1D_2$ line indeed resembles the behavior of the radiative K-L RRS of Mn across the K absorption edge in $KMnO_3$ [66], except for discrete features. The evolution of inelastic x-ray scattering into fluorescence across the K and L edges of free atoms [67,77], is also very similar.

The behavior of $I_c(\varepsilon_A,\omega_0)$ as a function of ε_A, as extracted from Fig. 5, can be qualitatively understood by examining Eq. (15). For $E_{\rm exc}<0$ and $\varepsilon>0$, we have $x\gg\Gamma_{1s}$. The asymmetric shape of the RRS profile is thus determined by the combined Lorentzian-tail and photoionization cross section factor $\sigma(x+E_{\rm exc})/x^2$, which increases rapidly as x decreases. Since $dN_f/d\varepsilon_A$ peaks at $x\simeq\varepsilon_A^0-\varepsilon_A$, the RRS intensity thus increases as a function of ε_A until it reaches $\varepsilon_A\simeq E_{\rm exc}+\varepsilon_A^0$. This edge, the energy of which disperses linearly with $E_{\rm exc}$, is rounded off by $dN_f/d\varepsilon_A$ and $N(E_{\rm exc}-E_{\rm exc}^0)$. Because $x\simeq -E_{\rm exc}\gg\Gamma_{1s}$, the shape of the edge is not influenced appreciably by the 1*s* lifetime. As $E_{\rm exc}$ approaches zero from below, the distribution (14) narrows and eventually evolves into the K-$L_{2,3}L_{2,3}$ $^1D_2$ line with total width $\Gamma=\Gamma_{1s}+\Gamma_{2p2p}$. According to Eq. (14), this feature follows because $I_c(\varepsilon_A,\omega_0)$ becomes a convolution of two Lorentzians associated with Γ_{1s} and Γ_{2p2p}, respectively. The influence of $N(E_{\rm exc}-E_{\rm exc}^0)$ is absorbed into a factor containing $\sigma(x+E_{\rm exc})$ which becomes weakly dependent on x as $E_{\rm exc}$ becomes positive and large. If we define an apparent FWHM of the asymmetric RRS distribution $I(\varepsilon_A,\omega_0)$, this eventually narrows just below $E_{\rm exc}=0$, because Γ_{1s} does not fully contribute to the width until $E_{\rm exc}>0$ [cf. Eq. (14)]. Careful examination of our data seems to support this conclusion, in accordance with previous observations of both radiative [78] and radiationless [79] RRS.

The normal curve in Fig. 6(a) represents the integrated intensity (13). The close resemblance between the bulk absorption curve and the measured integrated intensity for $E_{\rm exc}>0$ [Fig. 6(b)] is in accord with Eq. (14) which shows that, after integration of ε_A, $I(\omega_0)$ becomes proportional to $\sigma_c(x+E_{\rm exc})$, but smeared out by both the spectral function $N(E_{\rm exc}-E_{\rm exc}^0)$ and the 1*s* lifetime factor $(x^2+\Gamma_{1s}^2/4)^{-1}$.

(b) Resonance satellite line. Resonant features of the RRS spectrum have been associated with so-called white lines in the corresponding absorption spectrum of solids [33,66] or excitations to Rydberg states of free atoms [67,77]. White lines usually are strong, isolated absorption peaks in the vicinity of an inner-shell threshold; they are associated with formation of localized states of various types in the solid.

The main resonance features of radiationless RRS can be described with reference to Eq. (9). The assumption is that, for a given discrete final state $|\varepsilon'\rangle$, there is an isolated discrete state $|\tau'\rangle$ in the manifold of $|\tau\rangle$ such that $\langle\varepsilon'|\tau'\rangle$ is close to unity, but small for any other choice of $|\tau\rangle$. If we ignore recapture [75] to the state $|\varepsilon'\rangle$, we find

$$I_r(\varepsilon_A,\omega_0)=\int_{-I_{1s}}^{\infty}\frac{\Gamma(\varepsilon_A)\Gamma_r(\varepsilon')N(E_{\rm exc}-E_{\rm exc}^0)(\Gamma_{2p2p}/2\pi)dE_{\rm exc}}{[(\varepsilon'-E_{\rm exc})^2+\Gamma_{1s}^2/4][(\varepsilon_A-\varepsilon_A^0+\varepsilon'-E_{\rm exc})^2+\Gamma_{2p2p}^2/4]} \tag{15}$$

by using the approximation $\langle\varepsilon'|\tau'\rangle=\delta_{\varepsilon'\tau'}$ in Eq. (9). In Eq. (15), the excitation probability from the ground state to the excited state $|\varepsilon'\rangle$ is given by $\Gamma_r(\varepsilon')=(4\pi\alpha/3)(\varepsilon'+I_{1s})|\langle\varepsilon'\|r\|0\rangle|^2$.

If we set $N(E_{\rm exc}-E_{\rm exc}^0)=\delta(E_{\rm exc}-E_{\rm exc}^0)$, it follows from Eq. (15) that the shape of $I_r(\varepsilon_A,\omega_0)$ is not at all influenced by the 1*s* lifetime, only by the final double-2*p*-hole lifetime. This result demonstrates how use of a narrow incident-photon spectral function suppresses the effect of the intermediate-state lifetime width, in accordance with the analysis in Sec. IV A of the width of the resonance satellite line.

The narrow width of the integrated-intensity curve shown in Fig. 6(a) can also be explained through Eq. (15). Integration of Eq. (15) over ε_A affects only the final-state lifetime function $dN_f/d\varepsilon_A$ because $\Gamma(\varepsilon_A)$ is practically constant within the range of significant ε_A values. The integration results in a factor of unity, while $I_r(\omega_0)$ [Eq. (13)] becomes a convolution of the Gaussian $N(E_{\rm exc}-E_{\rm exc}^0)$, of width Γ_G, with the Lorentzian 1*s* lifetime function. Thus we can easily estimate the width of the resulting Voigt function from $\Gamma_G=0.69\pm0.02$ eV and $\Gamma_{1s}=0.53$ eV [Sec. III B]. The result is 1.02 eV, which is somewhat less than the measured width $\Gamma_r'=1.6\pm0.5$ eV. This difference indicates that the localized state $|\varepsilon'\rangle$ is subject to an intrinsic solid-state broadening associated with the localized part of the conduction band.

As discussed in connection with Eqs. (13), (14), and (15), the sum $I(\omega_0)=I_c(\omega_0)+I_r(\omega_0)$ should represent the K absorption spectrum. This result is in accordance with

Fig. 6(b), which shows the close resemblance between the K-$L_{2,3}L_{2,3}$ $^1D_2$ electron emission signal across the K edge and the *bulk* K absorption spectrum. This also indicates that it is quite adequate to neglect any interference terms between the continuous and discrete excitations, even though such terms are present in principle if the complete summation over intermediate one-electron states $|\tau\rangle$ is retained in Eq. (9).

Since the maximum of $dN_f/d\varepsilon_A$ follows the linear dispersion law $\varepsilon_a = E_{\rm exc} - \varepsilon' + \varepsilon_A^0$, it is also clear why a straight line of unit slope fits the data so well in Fig. 6(c). From Eq. (10) it is hence possible to interpret the most salient features of the P K-LL two-component structure as a function of both ε_A and ω_0. The result shows that RRS provides a unique means to detect bound excitonlike features in absorption spectra which do not otherwise exhibit any pronounced white lines in the threshold region. This result stands in contrast with the evolution of $L_{2,3}$-$M_{4,5}M_{4,5}$ ^1G electron emission of Rh and Pd across the $L_{2,3}$ edge, which exhibits a pronounced white line for both metals [33]. Rh and Pd also exhibit a much higher ratio of resonant to normal Auger intensities [33], related to the fact that states (referred to as the d band) near the bottom of the conduction band of these solids are much more localized than the corresponding states (with s-p hybridization character) in InP.

V. CONCLUSION

The evolution of K-$L_{2,3}L_{2,3}$ $^1D_2$ radiationless resonant Raman scattering into the corresponding Auger line of P in InP is found to be in accordance with the time-independent resonant scattering theory of inner-shell threshold phenomena.

The presence of a quasi-bound-state resonance in the Raman scattering of P reveals an excitation of a 1s electron to a quasi bound state in the bulk-sensitive P K absorption spectrum. The Raman resonance can be viewed approximately as a simultaneous excitation of a 2p electron into the half-filled 3p shell of P and of another 2p electron into the continuum. The coexistence of the discrete and continuous features in both spectra at the K edge is a consequence of screening that involves extra-atomic relaxation.

Analysis of above-threshold K-$L_{2,3}L_{2,3}$ and K-LV Auger spectra in combination with the K photoelectron spectrum of P shows that the multiplet splitting and lifetime widths are properties of predominantly atomic character. On the other hand, joint measurements of the Auger and photoelectron energies are found to yield accurate extra-atomic relaxation energies in accordance with earlier work.

The present results indicate that synchrotron-radiation-excited resonant Raman spectrometry can be a useful tool to study the response of valence electrons to the creation of core holes in semiconductor materials.

ACKNOWLEDGMENTS

We thank B. A. Karlin for expert technical assistance at NSLS and G. Materlik for helpful discussions and communicating his group's results in advance of publication. In the University of Oregon, this work was supported in part by the National Science Foundation through Grant No. PHY-9203779. In the Lawrence Livermore National Laboratory, the research was performed under the auspices of the U.S. Department of Energy under Contract No. W-7405-Eng-48. The National Synchrotron Light Source at Brookhaven National Laboratory, Upton, NY is supported by the U.S. Department of Energy (Division of Materials Sciences and Division of Chemical Sciences of the Office of Basic Energy Sciences) under Contract No. DE-AC02-76CH00016. The Stanford Synchrotron Radiation Laboratory is operated by the U.S. Department of Energy, Division of Chemical Sciences of the Office of Basic Energy Sciences.

[1] V. Schmidt, Rep. Prog. Phys. **55**, 1483 (1992), and references therein.

[2] M. Ya. Amusia, *Atomic Photo Effect* (Plenum, New York, 1990).

[3] R. L. Martin and D. A. Shirley, in *Electron Spectroscopy: Theory, Techniques, and Applications,* edited by C. R. Brundle and A. D. Baker (Academic, New York, 1977), Vol. I, Chap. 2, Sec. VIC, and references therein.

[4] See, for example, M. Cardona and L. Ley, in *Photoemission in Solids I: General Principles,* edited by M. Cardona and L. Ley (Springer, Berlin, 1978), Chap. 1; D. A. Shirley, *ibid.* Chap. 4.

[5] N. D. Lang and A. R. Williams, Phys. Rev. B **20**, 1369 (1979); see also C. D. Wagner, Faraday Discuss Chem. Soc. **60**, 291 (1975).

[6] B. Johansson and N. Mårtensson, Phys. Rev. B **21**, 4427 (1980).

[7] S. Aksela, R. Kumpula, H. Aksela, J. Väyrynen, R. M. Nieminen, and M. Puska, Phys. Rev. B **23**, 4362 (1981); S. Aksela, R. Kumpula, H. Aksela, and J. Väyrynen, Phys. Scr. **25**, 43 (1982).

[8] M. Ohno and G. Wendin, J. Phys. C **15**, 1787 (1982); S. L. Sorensen, S. J. Schaphorst, S. B. Whitfield, B. Crasemann, and R. Carr, Phys. Rev. A **44**, 350 (1991).

[9] F. P. Larkins, At. Data Nucl. Data Tables **20**, 311 (1977); J. Phys. C **10**, 2461 (1977); J. Phys. B **10**, 2453 (1977).

[10] U. Becker, in *X-Ray and Inner-Shell Processes,* edited by T. A. Carlson, M. O. Krause, and S. T. Manson, AIP Conf. Proc. No. 215 (AIP, New York, 1990), p. 621.

[11] T. Åberg and B. Crasemann, in *X-Ray Anomalous (Resonance) Scattering: Theory and Experiment,* edited by K. Fischer, G. Materlik, and C. Sparks (Elsevier/North-Holland, Amsterdam, 1994); see also B. Crasemann, Comments At. Mol. Phys. **22**, 163 (1989); T. Åberg, Phys. Scr. **T41**, 71 (1992).

[12] For a recent review see B. Crasemann, in *Electronic and Atomic Collisions,* edited by W. R. MacGillivray, I. E. McCarthy, and M. C. Standage (Hilger, Bristol, 1992), p. 69.

[13] W. Mehlhorn, in *Atomic Inner-Shell Physics,* edited by B. Crasemann (Plenum, New York, 1985), Chap. 4.

[14] *Proceedings of the 2nd International Workshop on Auger Spectroscopy and Electronic Structure (IWASES-II),* edited by K. Wandelt, C.-O. Almbladh, and R. Nyholm [Phys.

Scr. **T41**, 1 (1992)].
[15] T. Åberg and G. Howat, in *Corpuscles and Radiation in Matter I,* edited by S. Flügge and W. Mehlhorn, Handbuch der Physik Vol. XXXI (Springer, Berlin, 1982), p. 469.
[16] H. Aksela, S. Aksela, and N. Kabachnik, in *VUV and Soft X-Ray Photoionization Studies,* edited by U. Becker and D. A. Shirley (Plenum, New York, 1993), Chap. 10.
[17] I. Nenner and J. A. Beswick, in *Handbook on Synchrotron Radiation,* edited by G. V. Marr (North-Holland, Amsterdam, 1987), Vol. 2, Chap. 6.
[18] S. Svensson and L. Karlsson, Phys. Scr. **T41**, 132 (1992).
[19] T. X. Carroll and T. D. Thomas, J. Chem. Phys. **92**, 7171 (1990); M. Neeb, J.-E. Rubensson, M. Biermann, W. Eberhardt, K. J. Randall, J. Feldhaus, A. L. D. Kilcoyne, A. M. Bradshaw, Z. Xu, P. D. Johnson, and Y. Ma, Chem. Phys. Lett. **212**, 205 (1993); S. J. Schaphorst, C. D. Caldwell, M. O. Krause, and J. Jiménez-Mier, *ibid.* **213**, 315 (1993).
[20] D. E. Ramaker, Phys. Scr. **T41**, 77 (1992).
[21] D. A. Shirley, in *Photoemission in Solids I: General Principles,* edited by M. Cardona and L. Ley (Springer, Berlin, 1978), Chap. 4.
[22] M. Schärli and J. Brunner, Z. Phys. B **42**, 285 (1981).
[23] R. G. Cavell and R. N. S. Sodhi, J. Electron Spectrosc. Relat. Phenom. **41**, 25 (1986).
[24] V. I. Nefedov, V. G. Yarzhemsky, A. V. Chuvaev, and E. M. Trishkina, J. Electron Spectrosc. Relat. Phenom. **46**, 381 (1988).
[25] C. X. Yan and R. G. Cavell, J. Electron Spectrosc. Relat. Phenom. **42**, 49 (1987).
[26] R. Franke, Th. Chassé, P. Streubel, and A. Meisel, J. Electron Spectrosc. Relat. Phenom. **56**, 381 (1991).
[27] P. Streubel, R. Franke, Th. Chassé, R. Fellenberg, and R. Szargan, J. Electron Spectrosc. Relat. Phenom. **57**, 1 (1991).
[28] T. Chassé, R. Franke, P. Streubel, and A. Meisel, Phys. Scr. **T41**, 281 (1992).
[29] T. Chassé, R. Franke, C. Urban, R. Franzheld, P. Streubel, and A. Meisel, J. Electron Spectrosc. Relat. Phenom. **62**, 287 (1993).
[30] P. O. Nilsson and S. P. Svensson, Solid State Commun. **79**, 191 (1991).
[31] L. Calliari, M. Sancrotti, L. Duò, R. Cosso, P. Weightman, and F. Manghi, Phys. Scr. **T41**, 259 (1992).
[32] M. Elango, A. Ausmees, A. Kikas, E. Nömmiste, R. Ruus, A. Saar, J. F. van Acker, J. N. Anderesen, R. Nyholm, and I. Martinson, Phys. Rev. B **47**, 11 736 (1993).
[33] W. Drube, A. Lessman, and G. Materlik, in *X-Ray Anomalous (Resonance) Scattering* (Ref. [11]).
[34] J. C. Phillips, Rev. Mod. Phys. **42**, 317 (1970).
[35] W. A. Harrison, *Electronic Structure and the Properties of Solids* (Freeman, San Francisco, 1980).
[36] P. L. Cowan, S. Brennan, R. D. Deslattes, A. Henins, T. Jach, and E. G. Kessler, Nucl. Instrum. Methods Phys. Res. Sect. A **246**, 154 (1986); P. L. Cowan, S. Brennan, T. Jach, D. W. Lindle, and B. A. Karlin, Rev. Sci. Instrum. **60**, 1603 (1989).
[37] J. Cerino, J. Stöhr, N. Hower, and R. Z. Bachrach, Nucl. Instrum. Methods **172**, 227 (1980).
[38] J. C. Woicik, B. B. Pate, and P. Pianetta, Phys. Rev. B **39**, 8593 (1989).
[39] T. Kendelewicz, K. Miyano, R. Cao, J. C. Woicik, I. Lindau, and W. E. Spicer, Surf. Sci. **220**, L726 (1989).
[40] H. Körber and W. Mehlhorn, Z. Phys. **191**, 217 (1966).
[41] M. O. Krause, F. A. Stevie, L. J. Lewis, T. A. Carlson, and W. E. Moddeman, Phys. Lett. **31A**, 81 (1970); and comment thereon by T. A. Carlson, in *Proceedings of the International Conference on Inner-Shell Ionization Phenomena and Future Applications,* edited by R. W. Fink, S. T. Manson, J. M. Palms, and P. Venugopala Rao, U.S. Atomic Energy Commision Report No. CONF-720404 (National Technical Information Service, Springfield, VA, 1973), p. 2274.
[42] D. Chattarji, *The Theory of Auger Transitions* (Academic, New York, 1976), Chap. 5.
[43] C. D. Caldwell and M. O. Krause, Phys. Rev. A **47**, 759 (1993).
[44] I. P. Grant, B. J. McKenzie, P. H. Norrington, D. F. Mayers, and N. C. Pyper, Comput. Phys. Commun. **21**, 207 (1980).
[45] M. H. Chen, Phys. Rev. A **31**, 1449 (1985).
[46] J. B. Mann and W. R. Johnson, Phys. Rev. A **4**, 41 (1971).
[47] M. H. Chen, B. Crasemann, N. Mårtensson, and B. Johansson, Phys. Rev. A **31**, 556 (1985).
[48] S. J. Schaphorst, A. F. Kodre, J. Ruscheinski, B. Crasemann, T. Åberg, J. Tulkki, M. H. Chen, Y. Azuma, and G. S. Brown, Phys. Rev. A **47**, 1953 (1993).
[49] K. Siegbahn, C. Nordling, G. Johansson, J. Hedman, P. F. Hedén, K. Hamrin, U. Gelius, T. Bergmark, L. O. Werme, R. Manne, and Y. Baer, *ESCA Applied to Free Molecules* (North-Holland, Amsterdam, 1969).
[50] L. Asplund, P. Kelfve, B. Blomster, H. Siegbahn, and K. Siegbahn, Phys. Scr. **16**, 268 (1977).
[51] M. H. Chen and B. Crasemann, Phys. Rev. A **8**, 7 (1973).
[52] V. O. Kostroun, M. H. Chen, and B. Crasemann, Phys. Rev. A **3**, 533 (1971).
[53] J. H. Scofield, Phys. Rev. A **10**, 1507 (1974).
[54] A. Moljk, in *Proceedings of the International Conference on Inner-Shell Ionization Phenomena and Future Applications* (Ref. [41]).
[55] M. O. Krause, in *Atomic Inner-Shell Processes,* edited by B. Crasemann (Academic, New York, 1975), Vol. II, p. 33.
[56] G. K. Wertheim and S. B. DiCenzo, J. Electron Spectrosc. Relat. Phenom. **37**, 57 (1985).
[57] P. W. Palmberg, J. Vac. Sci. Technol. **12**, 379 (1975).
[58] C. N. Berglund and W. E. Spicer, Phys. Rev. **136**, A1030 (1964).
[59] M. O. Krause and J. H. Oliver, J. Phys. Chem. Ref. Data **8**, 329 (1979).
[60] M. H. Chen, B. Crasemann, and H. Mark, At. Data Nucl. Data Tables **24**, 13 (1979).
[61] M. H. Chen, B. Crasemann, and H. Mark, Phys. Rev. A **24**, 177 (1981).
[62] J. H. Scofield, At. Data Nucl. Data Tables **14**, 121 (1974).
[63] T. Kendelewicz, P. H. Mahowald, K. A. Bertness, C. E. McCants, I. Lindau, and W. E. Spicer, Phys. Rev. B **36**, 6543 (1987).
[64] W. G. Wilke, V. Hinkel, W. Theis, and K. Horn, Phys. Rev. B **40**, 9824 (1989).
[65] T. Åberg, Phys. Scr. **21**, 495 (1980).
[66] J. Tulkki and T. Åberg, J. Phys. B **15**, L435 (1982).
[67] T. Åberg and J. Tulkki, in *Atomic Inner-Shell Physics* (Ref. [13]), Chap. 10.
[68] P. Cowan, in *X-Ray Anomalous (Resonance) Scattering: Theory and Experiment* (Ref. [11]).
[69] G. B. Armen, T. Åberg, J. C. Levin, B. Crasemann, M. H.

Chen, G. E. Ice, and G. S. Brown, Phys. Rev. Lett. **54**, 1142 (1985).
[70] A. Kivimäki, A. Naves de Brito, S. Aksela, H. Aksela, O.-P. Sairanen, A. Ausmees, S. J. Osborne, L. B. Dantas, and S. Svensson, Phys. Rev. Lett. **71**, 4307 (1993).
[71] T. Åberg and J. L. Dehmer, J. Phys. C **6**, 1450 (1973).
[72] J. Valjakka, J. Utrianinen, T. Åberg, and J. Tulkki, Phys. Rev. B **32**, 6892 (1985).
[73] A. Meisel, G. Leonhardt, and P. Szargan, *X-Ray Spectra and Chemical Binding* (Springer, Berlin, 1989).
[74] J. Tulkki, T. Åberg, S. B. Whitfield, and B. Crasemann, Phys. Rev. A **41**, 181 (1990).
[75] S. B. Whitfield, J. Tulkki, and T. Åberg, Phys. Rev. A **44**, 6983 (1991).
[76] J. Tulkki,G. B. Armen, T. Åberg, B. Crasemann, and M. H. Chen, Z. Phys. D **5**, 241 (1987).
[77] M. A. MacDonald, S. H. Southworth, J. C. Levin, A. Henins, R. D. Deslattes, T. LeBrun, Y. Azuma, P. L. Cowan, and B. A. Karlin (unpublished); S. H. Southworth, Nucl. Instrum. Methods Phys. Res. Sect. B **87**, 247 (1994).
[78] P. Eisenberger, P. M. Platzman, and H. Winick, Phys. Rev. Lett. **36**, 623 (1976).
[79] G. S. Brown, M. H. Chen, B. Crasemann, and G. E. Ice, Phys. Rev. Lett. **45**, 1937 (1980).

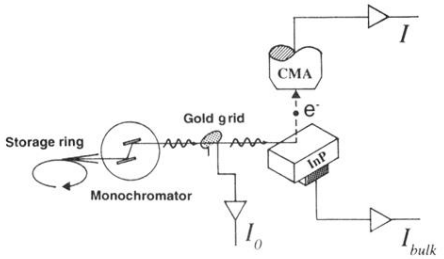

FIG. 1. Experimental layout for measuring electron spectra by recording the CMA current I in the pulse-counting mode. Bulk-sensitive absorption spectra were measured by recording the sample current I_{bulk}; surface-sensitive absorption was measured by recording I with the CMA set on L-VV Auger electrons. Results were normalized to the total photon flux proportional to the grid current I_0.